

# Super-resolution imaging via spatiotemporal frequency shifting and coherent detection

Leonid Alekseyev<sup>1</sup>, Evgenii Narimanov<sup>1</sup>, and Jacob Khurgin<sup>2</sup>

<sup>1</sup> *Department of Electrical and Computer Engineering,  
Purdue University, West Lafayette, IN 47907*

<sup>2</sup> *Department of Electrical and Computer Engineering,  
Johns Hopkins University, Baltimore, MD 21218*  
[evgenii@purdue.edu](mailto:evgenii@purdue.edu)

**Abstract:** Diffraction limit is manifested in the loss of high spatial frequency information that results from decay of evanescent waves. As a result, conventional far-field optics yields no information about an object's subwavelength features. Here we propose a novel approach to recovering evanescent waves in the far field, thereby enabling subwavelength-resolved imaging and spatial spectroscopy. Our approach relies on shifting the frequency and the wave vector of near-field components via scattering on acoustic phonons. This process effectively removes the spatial frequency cut-off for unambiguous far field detection. This technique can be adapted for digital holography, making it possible to perform phase-sensitive subwavelength imaging. We discuss the implementation of such a system in the mid-IR and THz bands, with possible extension to other spectral regions.

© 2022 Optical Society of America

**OCIS codes:** 230.1040 Acousto-optical devices; 300.6340 Spectroscopy, infrared

---

## References and links

1. M. E. Testorf and M. A. Fiddy, "Superresolution Imaging Revisited," *Advances in Imaging and Electron Physics* **163**, 165–218 (2010).
2. W. Lukosz, "Optical Systems with Resolving Powers Exceeding the Classical Limit II," *Journal of the Optical Society of America* **57**, 932 (1967).
3. Y. Kuznetsova, A. Neumann, and S. R. Brueck, "Imaging interferometric microscopy—approaching the linear systems limits of optical resolution." *Optics express* **15**, 6651–63 (2007).
4. M. G. L. Gustafsson, "Nonlinear structured-illumination microscopy: wide-field fluorescence imaging with theoretically unlimited resolution." *Proceedings of the National Academy of Sciences of the United States of America* **102**, 13,081–6 (2005).
5. M. Paturzo, F. Merola, S. Grilli, S. De Nicola, a. Finizio, and P. Ferraro, "Super-resolution in digital holography by a two-dimensional dynamic phase grating," *Optics Express* **16**, 17,107 (2008).
6. S. Durant, Z. Liu, J. M. Steele, and X. Zhang, "Theory of the transmission properties of an optical far-field superlens for imaging beyond the diffraction limit," *Journal of the Optical Society of America B* **23**, 2383 (2006).
7. B. Draznea, J. Preusser, J. M. Szarko, S. R. Leone, and W. D. J. Hinsberg, "Pattern characterization of deep-ultraviolet photoresists by near-field infrared microscopy," *J. Vac. Sci. Technol. B* **19**, 142–152 (2001).
8. B. Knoll and F. Keilmann, "Near-field probing of vibrational absorption for chemical microscopy," *Nature* **399**, 134–137 (1999).
9. N. C. J. van der Valk and P. C. M. Planken, "Electro-optic detection of subwavelength terahertz spot sizes in the near field of a metal tip," *Appl. Phys. Lett.* **81**, 1558–1560 (2002).
10. D. Mendlovic, A. W. Lohmann, N. Konforti, I. Kiryuschev, and Z. Zalevsky, "One-dimensional superresolution optical system for temporally restricted objects," *Applied Optics* **36**, 2353 (1997).

11. A. Shemer, D. Mendlovic, Z. Zalevsky, J. Garcia, and P. Garcia Martinez, "Superresolving Optical System with Time Multiplexing and Computer Decoding," *Applied Optics* **38**, 7245 (1999).
  12. R. W. Boyd, *Nonlinear Optics* (Academic Press, San Diego, 2003), 2nd ed.
  13. A. Korpel, *Acoustooptics* (Marcel Dekker, New York, 1989).
  14. R. Lanz and P. Muralt, "Bandpass filters for 8 ghz using solidly mounted bulk acoustic wave resonators," *IEEE Transactions on Ultrasonics, Ferroelectrics and Frequency Control* **52**, 938 – 948 (2005).
  15. M. B. Assouar, O. Elmazria, P. Kirsch, P. Alnot, V. Mortet, and C. Tiusan, "High-frequency surface acoustic wave devices based on aln/diamond layered structure realized using e-beam lithography," *Journal of Applied Physics* **101**, 114507 (2007).
  16. V. A. Podolskiy and E. E. Narimanov, "Near-sighted superlens," *Opt. Lett.* **30**, 75–77 (2005).
  17. N. I. Zheludev, "What diffraction limit?" *Nature materials* **7**, 420–2 (2008).
  18. J. W. Goodman and R. W. Lawrence, "Digital image formation from electronically detected holograms," *Applied Physics Letters* **11**, 77–79 (1967).
  19. U. Schnars and W. Jüptner, "Direct recording of holograms by a ccd target and numerical reconstruction," *Applied Optics* **33**, 179181 (1994).
  20. E. Cuche, P. Marquet, and C. Depeursinge, "Simultaneous amplitude-contrast and quantitative phase-contrast microscopy by numerical reconstruction of fresnel off-axis holograms," *Appl. Opt.* **38**, 6994–7001 (1999).
  21. S. Alexandrov, T. Hillman, T. Gutzler, and D. Sampson, "Synthetic Aperture Fourier Holographic Optical Microscopy," *Physical Review Letters* **97**, 168,102 (2006).
  22. C. Liu, Z. Liu, F. Bo, Y. Wang, and J. Zhu, "Super-resolution digital holographic imaging method," *Applied Physics Letters* **81**, 3143 (2002).
  23. F. Le Clerc, L. Collot, and M. Gross, "Numerical heterodyne holography with two-dimensional photodetector arrays," *Optics letters* **25**, 716–8 (2000).
  24. I. Yamaguchi and T. Zhang, "Phase-shifting digital holography," *Optics letters* **22**, 1268–70 (1997).
  25. J. B. Pendry, "Negative refraction makes a perfect lens," *Phys. Rev. Lett.* **85**, 3966–3969 (2000).
- 

## 1. Introduction

Microscopic imaging is the oldest and one of the most important non-invasive analysis techniques. It has been immensely successful in uncovering the structure, composition, and dynamics of micro- and nanoscale chemical and biological samples. Contemporary investigations in the life sciences demand ever-increasing resolution in a variety of spectral bands, with much attention given to IR and THz. This task is made complicated by the diffraction limit, which sets a fundamental upper bound on the maximum spatial frequency conveyed by conventional refractive optics.

Between the initial studies of optical resolution by Rayleigh and Abbe in the 19th century and the present day, a multitude of super-resolution systems and methods have been proposed and demonstrated [1]. Extracting information beyond the diffraction limit remains an active area of research. One general strategy for achieving sub-diffraction-limited images originates in the fact that it is possible to increase the spatial bandwidth of an optical system by sacrificing certain other characteristics (e.g. field of view, temporal bandwidth, acquisition time). This idea was pioneered by Lukosz in his seminal 1967 paper [2]. Indeed, many contemporary super-resolution techniques can be viewed as implementations of the Lukosz approach [1, 2], including off-axis illumination [3], structured illumination [4], spatial frequency-shifting gratings [5, 6], and even near-field scanning microscopy [7, 8, 9].

The idea of improving spatial resolution by using temporal degrees of freedom is particularly appealing for two reasons. First, time multiplexing can help resolve ambiguities that arise when high spatial frequencies are scattered into the optical passband, as in the case of evanescent waves diffracting off a subwavelength grating [6]. Second, in certain frequency bands outside the visible spectrum (e.g. far-IR or THz) it might be easier to manipulate signals in the time domain than in the spatial frequency domain. The potential utility of time-domain (or temporal-frequency domain) for super-resolution has long been recognized; in fact, a frequency-multiplexing scheme involving conjugate moving gratings was described in Lukosz's original paper [2] and demonstrated several decades later [10, 11]. However, owing to the complexity of the experimental setup, this scheme has not seen wide adoption.

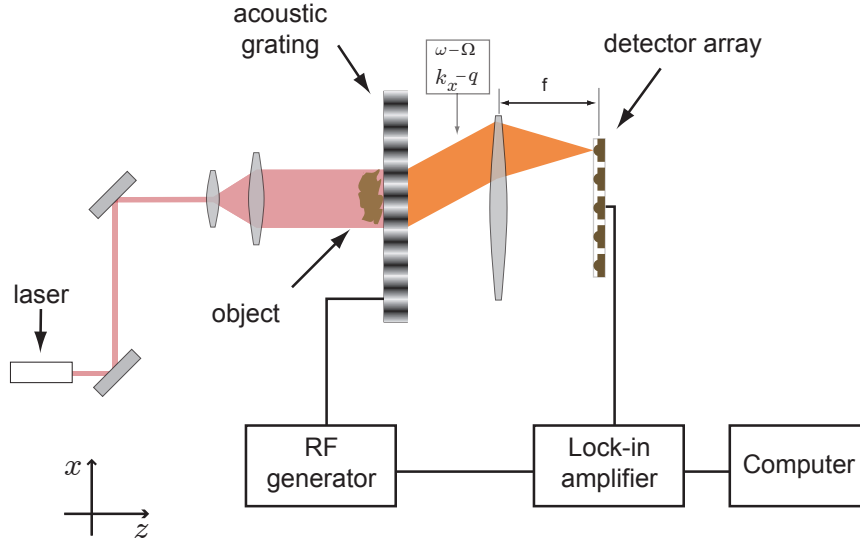


Fig. 1. Schematics of the proposed system.

In the present paper, we propose a time-multiplexed super-resolution system that requires no moving parts and is based on coherent detection of a frequency-shifted signal. This scheme lends itself particularly well to super-resolved imaging in IR and THz. Our approach is based on a device that converts evanescent waves to propagating waves via diffraction on acoustic phonons. The scattered and frequency-shifted waves can be easily decoupled from the existing propagating spectrum that forms the regular diffraction-limited image (thus, the image is free from aliasing). With minimal processing, these shifted components can be used to distinguish subwavelength features.

We will discuss two variations of this approach. Both rely on mixing the frequency-shifted fields scattered from the object with a reference wave, creating, at the detector, a beat note photocurrent which can be isolated through lock-in techniques. We will see that detection of high spatial frequencies is enabled by the spatial frequency offset of the scattered signal, and that a true super-resolved imaging configuration can be attained with an additional temporal frequency shift of the reference signal.

## 2. Scattering from a phonon grating: general description

The proposed super-resolution microscope/sensing system is shown in Fig. 1. The object is placed in the near field of an acousto-optic modulator (AOM) and illuminated with a plane wave from a mid-IR or THz source. Waves scattered from the object strike the phonon grating set up in the AOM by a running acoustic wave with frequency  $\Omega$ . Due to scattering on the phonons, the transverse wave vector  $k_x$  of the incident radiation is shifted by integer multiples of the phonon wave vector  $q$ , while its corresponding frequency is shifted by integer multiples of  $\Omega$ . For a sufficiently large  $q$ , the evanescent components of the object's spatial spectrum ( $|k_x| > \omega/c$ ) can be scattered into the propagating waves with  $|k'_x| \equiv |k_x - q| < \omega/c$ . The various spatial frequency components can be measured using a Fourier optics setup (e.g. a lens with a detector array in its focal plane).

We model our system by considering a rectangular sound column (i.e. planar acoustic wavefronts propagating in the  $x$  direction) interacting with a spectrum of incident plane waves in

a dielectric medium. We neglect the diffraction of the sound field or multiple reflections, and assume weak interaction. Due to photoelastic effect, the sound field produces a sinusoidal modulation of the dielectric permittivity [12],

$$\varepsilon(x) = \bar{\varepsilon} + \Delta\varepsilon \cos(qx - \Omega t), \quad (1)$$

which corresponds to a spatiotemporal volume grating. We may write the general form of the field inside the grating as a sum over the discrete diffracted orders,

$$E = \sum_j A_j(z) \exp[i(k_x + jq)x - i(\omega + j\Omega)t]. \quad (2)$$

The scattered plane wave components  $A_j(z)$  are then governed by the Raman-Nath equations [13],

$$A_j''(z) + k_{z_j}^2 A_j(z) = -\frac{\Delta\varepsilon}{2c^2} \omega_j^2 [A_{j-1}(z) + A_{j+1}(z)], \quad (3)$$

where  $k_{z_j} = \left[ \bar{\varepsilon} \frac{\omega^2}{c^2} - (k_x + jq)^2 \right]^{1/2}$ , and  $\omega_j \simeq \omega$ .

The amplitude of the  $j^{\text{th}}$  diffracted order,  $A_j$ , is proportional to  $(\Delta\varepsilon)^j$ , with  $\Delta\varepsilon/\varepsilon \ll 1$ , allowing to ignore higher order terms ( $j \geq 2$ ). We can, furthermore, conclude that the amount of energy scattered into the shifted waves is small, thereby permitting to neglect the variation of 0<sup>th</sup> diffracted order  $A_0$  (the undepleted pump approximation) [12]. We note that for propagating waves, this conclusion is valid insofar as there exists no Bragg matching between the incident and diffracted waves. Since the phonon wave vector  $q$  is a tunable parameter in our model, it is always possible to pick a range of  $q$  values to ensure minimal energy loss in the incident wave. For the evanescent waves, the undepleted pump approximation is justified by the small interaction length.

Keeping terms up to first order in Eq. (2), we obtain:

$$A_{\pm}''(z) + k_{z_{\pm}}^2 A_{\pm}(z) = -\frac{\Delta\varepsilon}{2c^2} \omega_j^2 A_0(z). \quad (4)$$

The scattering amplitudes of “upshifted” and “downshifted” waves can be obtained from this expression. Since the input field at spatial frequencies  $(k_x \mp q)$  contributes to the output field at spatial frequency  $k_x$ , we may write:

$$E_{\text{out}}(k_x) = [\tilde{A}_- \exp(i\Omega t) + \tilde{A}_+ \exp(-i\Omega t) + \tilde{A}_0] \exp[i(k_x x - \omega t)], \quad (5)$$

with  $\tilde{A}_{\pm} \equiv t^{\pm} E_{\text{in}}(k_x \mp q)$ ,  $\tilde{A}_0 \equiv t_0 E_{\text{in}}(k_x)$ . Scattering coefficients  $t^{\pm}$  are, for the case of evanescent waves, given by

$$t^{\pm} = t_0 \frac{\Delta\varepsilon}{2} \left( \frac{\omega}{c} \right)^2 \frac{1}{k_z^{\pm} \sqrt{(k_z^{\pm})^2 + \kappa^2}} \approx t_0 \frac{\Delta\varepsilon}{2} \left( \frac{\omega}{c} \right)^2 \frac{1}{k_z^{\pm} \sqrt{q(q \mp 2k_x)}}, \quad (6)$$

where  $k_z^{\pm} = \sqrt{\varepsilon(\omega/c)^2 - (k_x \mp q)^2}$ ,  $\kappa = ik_z = \sqrt{k_x^2 - \varepsilon(\omega/c)^2}$ , and  $t_0$  is a Fresnel transmission coefficient. We see that the conversion of incident evanescent waves into propagating signals depends critically on the acoustooptic index contrast  $\Delta\varepsilon$  and on the effective interaction length  $1/\kappa$ . We note, also, that Eq. (6) describes also the generation of shifted spatial frequencies for the case where the incident wave is propagating (provided we make the association  $\kappa = ik_z$ ). In this case, the divergence of Eq. (6) around  $q \approx 0$ , as well as  $q \approx \pm 2k_x$  signifies the breakdown of the perturbative treatment of Eq. (3) due to the onset of Bragg-matching.

From Eq. (6) we can estimate the diffraction efficiency of high spatial frequency input signal  $E_{\text{in}}(k_x^{\text{in}})$  as

$$|t^\pm| \approx \frac{\omega/c}{2k_x^{\text{in}}} \frac{\Delta\varepsilon}{n(1+n)}, \quad (7)$$

with  $n = \sqrt{\varepsilon}$  (the refractive index of the acoustic medium), and  $\Delta\varepsilon \propto \sqrt{F}$ , the flux of acoustic energy per unit area.

We thus obtain the amplitudes of the frequency-shifted waves. We define  $\tilde{A}_\pm = t^\pm E_{\text{in}}(k_x \mp q)$ ,  $\tilde{A}_0 = t_0 E_{\text{in}}(k_x)$  (with linear coefficients  $t_0$ ,  $t^\pm$  describing the generation of phonon-scattered and/or device transmission characteristics) and assume  $\tilde{A}_i \gg \tilde{A}_0 \gg \tilde{A}^\pm$ , where  $\tilde{A}_i$  is the detected amplitude of the illuminating wave  $A_i e^{ik_0 z}$ . Averaging out the signal over the finite detector aperture and subtracting the background (which can be done electronically), we can write the intensity detected by the system of Fig. 1 as

$$I_{\text{out}} = |\tilde{A}_0|^2 + 2 (|\tilde{A}_i \tilde{A}_-|^2 + |\tilde{A}_i \tilde{A}_+|^2)^{1/2} \cos(\Omega t + \gamma). \quad (8)$$

The two terms in this equation can be decoupled using standard techniques: the DC term is isolated with the aid of a low-pass filter, while the term oscillating at the acoustic frequency  $\Omega$  is recoverable using standard lock-in detection. For any given  $k_x$ , this second term contains contributions from both  $\tilde{A}_+ = t^+ E_{\text{in}}(k_x - q)$  and  $\tilde{A}_- = t^- E_{\text{in}}(k_x + q)$ . Although the coupling between these two quantities, together with the lack of phase information, makes it difficult to recover the spatial spectrum, the information collected can be used in detecting subwavelength morphological changes between different samples.

### 3. Super-resolved fingerprinting: numerical simulation

We now illustrate the ability of the proposed system to distinguished between subwavelength spatial features of different objects. In particular, we utilize Eq. (8) to perform a comparison between the standard optical target (USAF test chart) and a modified target, where the label of every 6th line group has been randomly replaced. The first replacement corresponds to the last resolvable line group ( $\lambda/2.5$  line separation); the subsequent replacements correspond to halving the size of the line groups ( $\lambda/5, \dots, \lambda/40$ ). We assume the measurement is performed by selecting an element of a photodetector array in the observation plane and using two orthogonal acoustic transducers to scan the acoustic wavevector within the range  $q_{x,y} \in [-25\omega/c, 25\omega/c]$ . (We choose these values with the aim to improve by a factor of  $\sim 20$  on the Abbe  $\lambda/2$  resolution limit, thereby collecting meaningful information about the  $\lambda/40$  line group.)

In our computations, we assume the operating wavelength of  $10 \mu\text{m}$  with germanium as the acoustic medium. We take  $\Delta\varepsilon = 10^{-3}$  and restrict the magnitude of the acoustic wave vector  $q$  to  $25\omega/c$ . Since for high spatial frequencies  $k_x^{\text{in}} \approx q$ , acoustic driving frequencies up to 8.75 GHz are required to retrieve  $k_x^{\text{in}} \approx 25\omega/c$ . These parameters are within reach of modern ultrasonic transducers [14], as well as surface acoustic wave devices [15].

It should be emphasized that any method that relies on digital processing of raw data can suffer from rapid – sometimes exponential [16] – accumulation of noise. (Indeed, some proposed super-resolution methods even stipulate the need for an exponentially strong input signal to overcome noise and losses [17].) To show that this is not the case here, in our computations we add a normally-distributed random term to the AC amplitude of Eq. (8) in order to simulate noise in the system. Because SNR is expected to be lowest for maximum values of the acoustic wavevector  $q$ , we consider SNR=10 for  $q = 25\omega/c$ <sup>1</sup>. Assuming a  $20 \times 20$  element photodetector array, we compute the signal given by Eq. (8) for the standard target, as well as the modified target [Fig. 2(a)]. Fig. 2(b) shows the result of subtracting the two datasets and performing an

<sup>1</sup>Acoustooptic diffraction efficiency, and hence the signal-to-noise ratio varies as  $1/q$ .

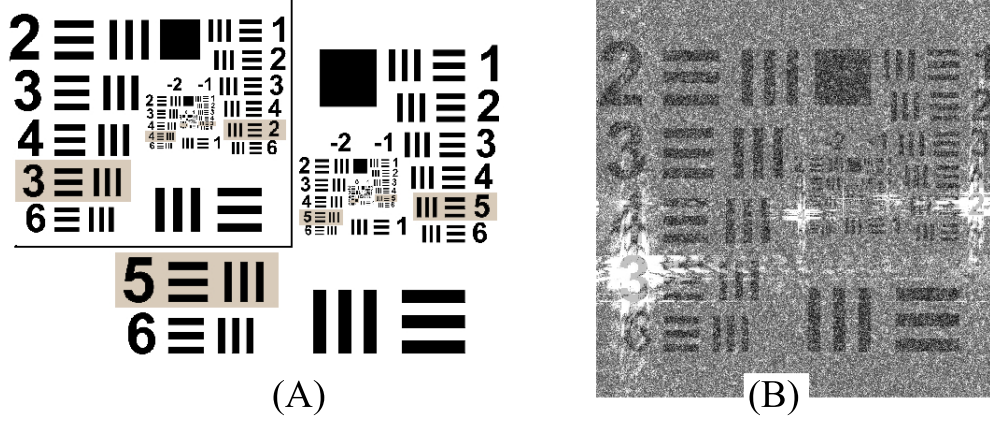


Fig. 2. (a) Optical test target and its modified version (inset). In the modified target, the “5” label of every column has been replaced by another digit. (b) Computed output of the system in the presence of noise (shown in grayscale) assuming a realistic, noisy detector with 400 active photocells. The modified optical target is superimposed for illustration purposes. The output of the system clearly identifies the location of every modified digit, even for regions far below the diffraction limit.

inverse Fourier transform, with the resulting plot superimposed onto the modified optical target. Evidently, every change in the original image is manifested in this difference diagram. Furthermore, it is largely localized in the vicinity of the actual changed pixels. It is possible to discern the difference signal even from the  $\lambda/40$  line group label.

The ability to distinguish between fine spatial features of optical targets makes the system described above uniquely suited for identifying objects based on their subwavelength spatial features. As a result, it may find applications in fingerprinting and/or detection of chemical and biological structures.

#### 4. Super-resolved digital holography

A straightforward modification of the setup described above not only allows to measure the “downshifted”  $\tilde{A}_-$  component directly, but also provides a method for retrieving phase information, making it possible to perform phase-contrast microscopy, and potentially enabling 3D imaging on subwavelength scales.

To this end, a portion of the illuminating radiation is shifted in frequency by  $\Omega_b$  using a second AOM. Unlike the modulator that interacts with light scattered from the sample in the Raman-Nath regime [12], this second AOM utilizes an appropriately oriented and longer cell to produce Bragg scattering. This results in a strong optical signal at frequency  $\omega + \Omega_b$ ,  $|\tilde{A}_b| \exp[i(k_b \cdot r - (\omega + \Omega_b)t)]$ , which is projected onto the detector [see Fig. 3(a)]. Interference between the two optical signals produces beat note photocurrents with frequencies  $\Omega$ ,  $\Omega_b$ ,  $\Omega_b + \Omega$ ,  $\Omega_b - \Omega$ :

$$I_{\text{out}}(k_x) = |E_i \exp(ik_0 z) + \tilde{A}_b \exp(ik \cdot r) + [\tilde{A}^- \exp(i\Omega t) + \tilde{A}^+ \exp(-i\Omega t) + \tilde{A}_0] \exp(ik \cdot r)|^2 \\ = \dots + 2|\tilde{A}^- \tilde{A}_b| \cos[(\Omega_b + \Omega)t + \Delta\Phi^-] + 2|\tilde{A}^+ \tilde{A}_b| \cos[(\Omega_b - \Omega)t + \Delta\Phi^+] + \dots, \quad (9)$$

where  $\Delta\Phi^\pm = (k_b - k) \cdot r - \phi^\pm$  is the phase difference between the signal from the Bragg cell,  $|\tilde{A}_b| \exp(ik_b \cdot r)$ , and the Raman-Nath-scattered signal  $\tilde{A}^\pm \exp(ik \cdot r) = |\tilde{A}^\pm| \exp[i(\phi^\pm + k \cdot r)]$ .

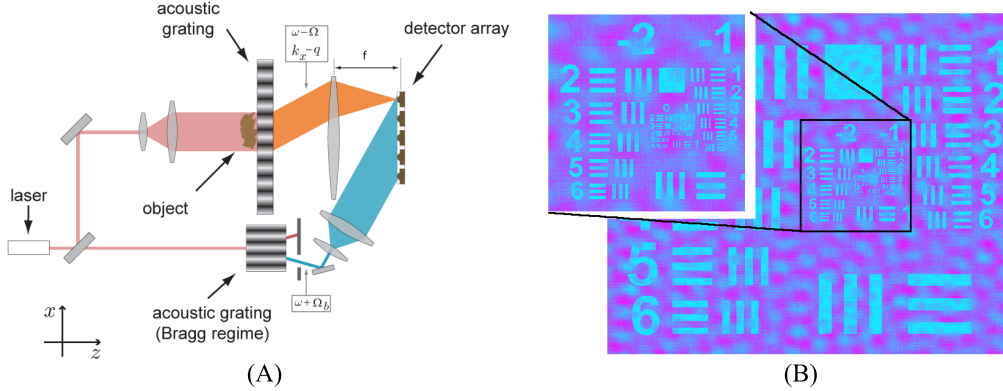


Fig. 3. (a) Schematics of the proposed system. Note the Bragg-shifted reference beam that aids in providing phase information. (b) The computed output of the system with optical test target as the object in the presence of noise.

Of special interest is the component at frequency  $\Omega + \Omega_b$ , which carries the high spatial frequency information contained in its modulus and its phase  $\Delta\Phi^- \simeq (k_x^b - k_x)x - \phi^-$ . Both of these quantities can be retrieved using lock-in techniques. To produce the lock-in reference, the RF signals driving the two acoustic cells can be mixed using a nonlinear element (e.g. a diode) and appropriately filtered to produce the sum frequency. As a result, complete information can be obtained about the complex high spatial frequency Fourier component  $\tilde{A}^-$ , from which it is straightforward to deduce the field  $E_{\text{in}}(k_x + q)$ . By collecting data from multiple CCD pixels, as well as by varying the acoustic wave vector  $q$ , information can be collected about the entire spatial spectrum of the object. The data can then be digitally processed to produce a spatial-domain image containing subwavelength details, as well as phase contrast.

Because the Bragg-shifted signal we use to decouple the  $\tilde{A}_+$  and  $\tilde{A}_-$  terms serves as a reference needed to record phase information, and because the image is reconstructed digitally, our technique belongs in the category of digital Fourier holography (DFH) [18, 19, 20]. However, the proposed coherent detection method is different from traditional DFH setups in that it effectively converts sample spatial frequencies to temporal ones. In conventional holography, care has to be taken to isolate the target signal both in real and Fourier space. This translates into limitation on the field of view, as well as maximum attainable resolution [20]. The requirement that the CCD pixel spacing must allow for imaging the reference wave fringes further limits the resolution. As a result, simple digital holography setups suffer from very narrow spatial frequency passbands (N.A.  $\sim 0.1$ ). Synthetic aperture techniques based on gratings [21, 22, 5] have been successfully shown to increase the effective numerical aperture, as has heterodyne detection [23]. Our method combines the benefits of these approaches: dynamic acoustic grating allows to scan the spatial frequency space while always remaining in the CCD's passband, while the temporal frequency shifts multiplex the data, effectively increasing the number of information channels in a given spatial frequency band.

We simulate the performance of the frequency-shifted digital holography system by first using Eq. (9) to compute the response of the system to a calibration signal having unit amplitude for all spatial frequencies. In practice, such calibration signal might be generated by placing a point source in the vicinity of the AOM. Eq. (9) also provides the effective amplitude and phase transfer functions that allow to determine the detected signal for a given input field distribution. Gaussian noise is added to simulate spurious signals in the system. The input signal can then be obtained by dividing out the calibration quantities. In Fig. 3(b) we plot the simulated retrieved

field magnitude. Zooming in on the central part of the test pattern (figure inset) it is evident that every line group is distinctly resolved, suggesting that the effective numerical aperture is  $> 1$  (due to reconstruction of evanescent waves).

## 5. Potential improvements of the proposed system and extension to higher frequencies

As demonstrated earlier, the resolution of the proposed systems will depend on many factors, including the maximum attainable frequency shift, integration time, acoustooptic index contrast, and success in minimizing detector noise, laser linewidth, and speckle. In addition to resolution improvement, there exist many possible ways to enhance the functionality and the performance of the proposed devices. For instance, because the phase information is preserved, the full complex field in the object plane can be reconstructed, potentially enabling 3D imaging via, e.g., phase-shifting interferometry [24]. On the performance front, the sensitivity of the device may be improved with a subwavelength layer of highly doped semiconductor at the front AOM facet. When the dielectric constant of this layer is equal to  $-1$ , the evanescent fields are strongly enhanced due to resonant coupling to surface plasmons in the doped layer (a phenomenon known as “poor-man’s superlensing” [25]), leading to better SNR at the detector. Another possible way to improve the scattering efficiency of evanescent waves is placing the sample directly in the path of an acoustic wave, for instance, by running the wave through a microchannel containing objects to be studied. This approach may find many applications in novel integrated biological/chemical detection devices.

Finally, we comment on the possibility of extending the proposed approach to frequencies other than the mid-IR and THz bands discussed here. While implementing the system for lower frequencies is essentially trivial, near-IR and optical frequencies pose a challenge. Acoustic phonon energies in practical devices do not approach the values necessary to produce a substantial wave vector shift in these spectral bands. However, the required shift in spatial and temporal frequencies can in principle be attained by replacing the acoustooptic medium with a nanostructured periodically moving grating. In this scenario, the spatial frequency shift is determined by the periodicity of the grating while the temporal frequency shift is determined by the speed of grating oscillation. These parameters can be adjusted independently to optimize performance.

## 6. Conclusion

We have proposed a system that enables detection of sub-diffraction-limited spatial spectrum components in the far field by utilizing scattering from an acoustic grating. This process works whenever the spatial frequencies of the object are comparable in scale to the acoustic wave vector. In its simplest implementation, the system could aid in “fingerprinting” of samples based on their subwavelength spatial features. With the use of an additional Bragg-shifted reference signal, it is also possible to recover the phase of the original optical signal. The proposed approach has the potential to greatly enhance the specificity of mid-IR and THz spectroscopy.

## Acknowledgements

This work was supported in part by United States Army Research Office (USARO) Multidisciplinary University Research Initiative program awards 50342-PH-MUR and W911NF-09-1-0539.